Journal of
*Marine Science and Engineering*

MDPI

*Article*

# Sediment Deposition Following Construction of a Breakwater Harbor: Point Judith Harbor of Refuge, Rhode Island, USA

**Bryan A. Oakley [1,*], Cody J. Murphy [1], Kym K. Lee [1], Robert J. Hollis [2], Brian Caccioppoli [3] and John W. King [3]**

[1] Department of Environmental Earth Science, Eastern Connecticut State University, Willimantic, CT 06226, USA; murphycod@my.easternct.edu (C.J.M.); leeky@my.easternct.edu (K.K.L.)
[2] Rhode Island Geological Survey, Kingston, RI 02881, USA; rhollis@appliedcoastal.com
[3] Graduate school of Oceanography, University of Rhode Island, Narragansett, RI 02882, USA; bcaccioppoli@uri.edu (B.C.); jwking@uri.edu (J.W.K.)
* Correspondence: OakleyB@easternct.edu; Tel.: +1-860-465-0418

Received: 9 October 2020; Accepted: 27 October 2020; Published: 31 October 2020


**Abstract:** Breakwaters are a common shoreline protection structure, often trapping sediment as the incoming wave energy is reduced. Quantifying the dynamics and volume of these sediment sinks within a coastal system is an important step toward understanding the sediment budget for a particular coastal area. This study examines the volume of sediment deposited within the breakwater enclosed Point Judith Harbor of Refuge (Rhode Island, United States of America (USA)) in the late 19th century using seismic reflection profiles, bathymetric mapping, and isotopic analysis of core sediment. Geophysical profiles show a district seismic facies up to 4 m thick above the ravinement surface, particularly in the western and central portion of the harbor. Century-scale bathymetric changes revealed shoaling of a similar magnitude, and isotopic data support the deposition of this sediment package within the 20th century. The total volume of sediment within the harbor exceeds $5.0 \times 10^6$ m$^3$, with an estimated sand volume of $3.6 \times 10^6$ m$^3$. The results show that the harbor is a substantial sediment sink for the Rhode Island South Shore and provide the basis for future studies of the sediment budget for this shoreline.

**Keywords:** harbor; sediment budget; sedimentation; seismic reflection

## 1. Introduction

The use of armoring to protect coastal properties from storm impact, erosion, and sea-level rise has increased markedly since 1900 [1]. Recent estimates are that 14% of the continual United States (US) shoreline has been armored, and that number could double by 2100 [1]. Shoreline protection structures alter the physical characteristics of a shoreline, affect sediment transport pathways, and can negatively impact the fronting beach and adjacent shorelines, both physically and ecologically [2–6]. Understanding the natural and anthropogenically influenced coastal sediment transport rates and pathways is a critical part of managing the shoreline behavior in a time of rising sea level [7] and the potential for increased storminess [8,9]. Breakwaters, either detached or shore-connected, are common shoreline protection structures, designed to reduce wave energy, providing a safe harbor and some protection of the shorelines and vessels behind the breakwater [2]. Sediment deposition behind these structures is expected as the incoming wave energy is reduced [10], and the volume of newly deposited sediment provides an estimate of the rate and direction of sediment transport, which is key to assessing the sediment budget in coastal systems. Sediment budgets remain one of the most useful concepts in coastal research and science-based coastal management [10] and can be used to quantify the volume

of sediment sources, sinks, and alongshore and cross-shore transport pathways for a given coastal segment [11]. Sediment budgets are typically based on the volume(s) of sediment that are the most well constrained within a system, and unknown or lesser known values can be approximated [12].

The Rhode Island South Shore (RISS) (Figure 1) has been described as "sediment-starved", with an estimated berm volume based on beach profiles of $1 \times 10^6$ m$^3$ [13] and less than $4 \times 10^6$ m$^3$ of modern (Holocene) sediment in the uppermost shoreface [14] along the entire 33 km shoreline. To date, no sediment budget exists for the RISS, and the rates and relative magnitude of the various sediment transport pathways remain poorly constrained. The RISS was included in a conceptual regional sediment budget [15], which depicted the general sediment budget as "stable" (i.e., neither erosional nor accretionary), although the authors reported low confidence in the results along the RISS on the basis of limited available data. The aim of this paper is to describe a significant sediment sink for the RISS identified within the Point Judith Harbor of Refuge (HoR), a jetty/breakwater-enclosed harbor, using high-resolution seismic reflection profiling, sediment coring, and historic bathymetric surveys (Figure 1). The hypothesis tested is that sediment accumulating above the transgressive ravinement surface unconformity [16] began immediately following the construction of the breakwaters. Quantifying total sediment deposition within the HoR represents an important step toward completing a sediment budget for the RISS, as well as understanding the influences of attached and detached breakwaters on sediment transport and deposition along a sediment-starved coastline.

## 2. Study Area

The HoR is located near the eastern end of the RISS (Figure 1), a 33 km long, microtidal (great diurnal range 1.03 m [17]), mixed-energy, wave-dominated coastline [18,19]. Fitzgerald and van Heteren [20] classified the RISS as a wave-dominated mainland-segmented barrier system, with headlands composed of glacial stratified deposits composed of sand and gravel, with till (diamict) separating barrier spits. The HoR consists of three breakwaters, with the western structure also functioning as a jetty for the Point Judith Pond inlet (Figure 1). Two entrances to the harbor are located between the eastern breakwater and central breakwater (known locally as the "East Gap") and between the western breakwater and central breakwater ("West Gap"). Construction of the breakwaters began in 1891. The central (main) breakwater was completed in 1898; the eastern and western breakwaters were completed in 1906 and 1914, respectively [21–23]. The enclosed harbor has a maximum depth of 10 m below mean lower low water (MLLW) [24]. The harbor has gone through various repairs and alterations over the past 60 years, and, while the structures have increased in elevation and width, they have not been lengthened [23]. Construction of the harbor was designed to provide a refuge for shipping traffic, to enable search and rescue operations, and to act as a commercial harbor and protection for the adjacent shoreline [23,25].

The shoreline within the HoR is a mixture of barrier and headland. The 1.6 km Sand Hill Cove barrier spit comprises the western portion of the HoR shoreline. The Point Judith headland forms the eastern end of the HoR (Figure 1) and is a combination of moraine deposits (a mixture of till and stratified deposits) and glacial stratified sand and gravel [26–28]. The tidal inlet within the HoR connects Block Island Sound to two coastal lagoons, Point Judith Pond and Potters Pond (called salt ponds in local terminology) (Figure 1). Long-term, nearshore wave observations here are limited; however, between July 2010 and July 2011, wave observations were recorded at a station 3 km west of the HoR (water depth 9.5 m) [29]. Over that period, significant wave heights ranged from 0–2.8 m, and wave heights were less than 1 m 83% of the time. Waves approached from the south-southeast (SSE) or south-southwest (SSW) 88% of the observed period [29]. Wave period ranged from 5–11 s [29]. These results are similar to the hindcast waves for the RISS, which report a mean significant wave height of 1 m, with an average period of 8 s [30]. Wave height observations at two stations in 10 m of water depth during Tropical Storm Irene (2011) yielded significant wave heights elsewhere within Block Island Sound of 4.1 m ($H_{max} > 6$ m), with a peak period of 10 s [29]. This is similar to modeled wave heights for the RISS, with heights of >7 m for a 10 year return period storm and >8 m for 100 year return period [30]. A lack of direct wave observations within the HoR limits quantification of

wave conditions or the reduction of incident wave energy within the harbor. Modeling studies show >50 % reduction in wave height relative to open ocean conditions, with higher wave energy entering the harbor through the eastern entrance [25]. Modeled wave heights during storms within the HoR were as high as 3.5 m near the east entrance and generally decreased toward the west [23]. Limited tidal current observations have been published for the HoR. Boothroyd et al. [31] reported strong flood asymmetry for tidal currents measured within the inlet channel to Point Judith Pond. Predictions of currents at the eastern entrance show a slight ebb dominance, with peak velocities >0.8 m·s$^{-1}$ [32].

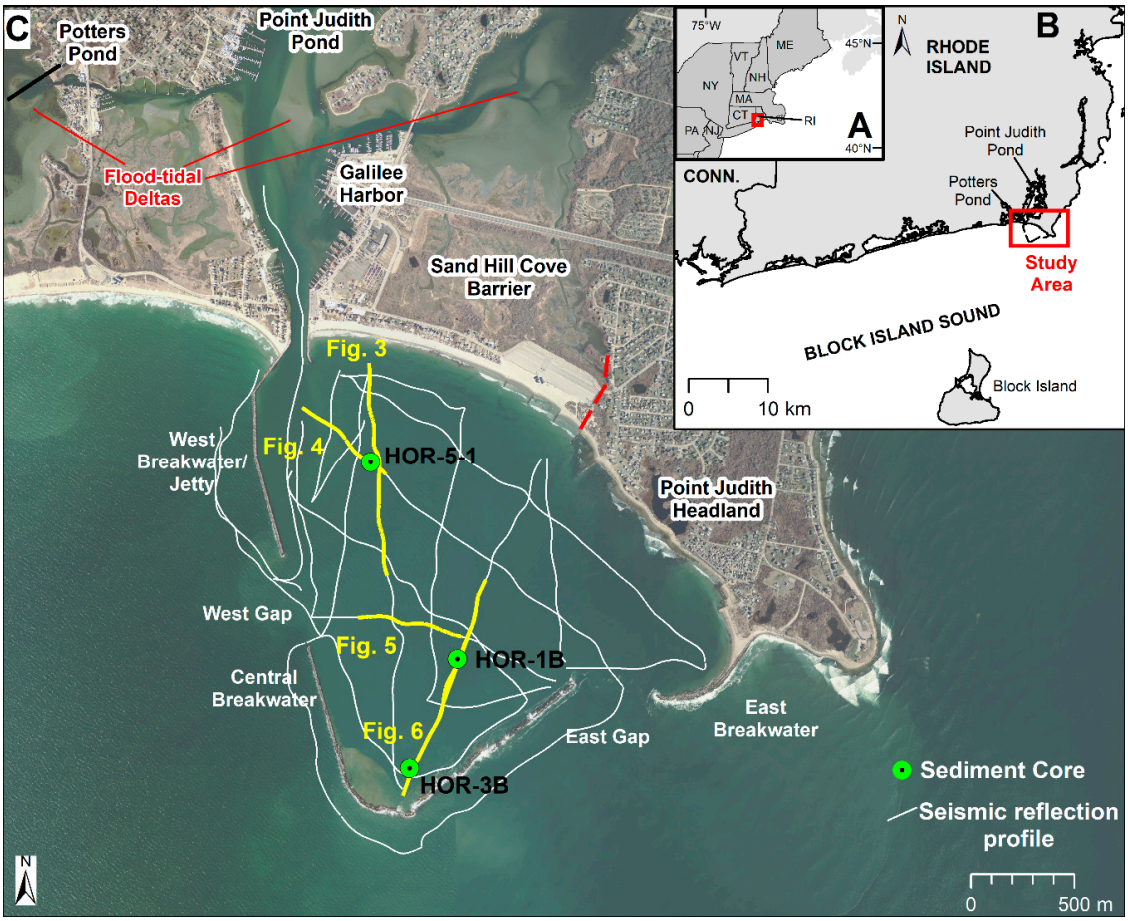


**Figure 1.** (**A**) Locus map of southern New England showing the location of the study area. (**B**) Location of the Point Judith Harbor of Refuge (HoR) relative to the rest of the Rhode Island South Shore. (**C**) 2014 orthophotograph of the HoR. White lines are the extent of 2016 and 2017 seismic reflection profiles. Yellow lines show the location of the seismic reflection profiles seen in Figures 4–7. Dashed red line shows the approximate boundary between the Sand Hill Cove Barrier and Point Judith Headland. Green circles show the location of sediment cores discussed in the text. Note the sand accumulations within Point Judith Pond and Potters Pond which represent flood-tidal delta deposition.

Vertical aerial photographs and digital orthophotographs were used to construct 1:2000 scale historic maps depicting shoreline change from 1939 to 2014 [33]. However, these maps postdate the construction of the breakwaters, but they show a period of shoreline progradation along the Sand Hill Cove Barrier between 1939 and 1963, with shoreline retreat up to 26 m between 1963 and 2014. Shoreline retreat in the eastern, headland portion of the HoR has been more systematic, with general recession since 1939 of 10–30 m. The exception is the area adjacent to the inside of the eastern breakwater, where the shoreline has prograded 50–90 m [33]. Some small segments of the shoreline show net accretion (1939–2014) of up to 10 m near the groin field at the east end of the Sand Hill Cove barrier. The US Geological Survey (USGS) shoreline change analysis [34] reported net accretion between

1970 and 2000 (mean +0.24 m·year$^{-1}$); however. this included Light Detection and Ranging (LiDAR) derived positions (AD 2000) substantially seaward of other mapped shorelines. The USGS report also included a shoreline from an 1872 T-sheet survey, which suggests that the western half of the HoR has experienced ~30 m of progradation between 1872 and 2014 with minor (<10 m) retreat in the eastern portion of the HoR.

Previous work using oblique aerial photographs, single-beam echosounder-derived bathymetry, and vibracores suggests that Point Judith Pond is a sediment sink, with $1.1 \times 10^4$ m$^3$·year$^{-1}$ of sediment deposited within the flood-tidal delta complex [31]. Approximately $4 \times 10^5$ m$^3$ of sediment has been dredged from the main channel and tidal delta complex within Point Judith Pond since 1950 (Michael Walsh, U.S. Army Corps of Engineers, Concord (Massachusetts), USA; pers. comm.). Recent studies focused on the condition of the breakwater's noted deposition at the apex of the central breakwater (visible in Figure 1), which they attributed to sediment transport via wave transmission through and over the top of the structure [25]. Mapping using side-scan sonar and sediment grab samples showed that the surface geology within the northwestern portion of the HoR is dominated by sand, with cobble to boulder gravel offshore of the Point Judith Headland in the northeastern HoR (Figure 2) [14,35]. Surface sediment samples from the inlet channel and adjacent tidal deltas consist of >90% sand [36].

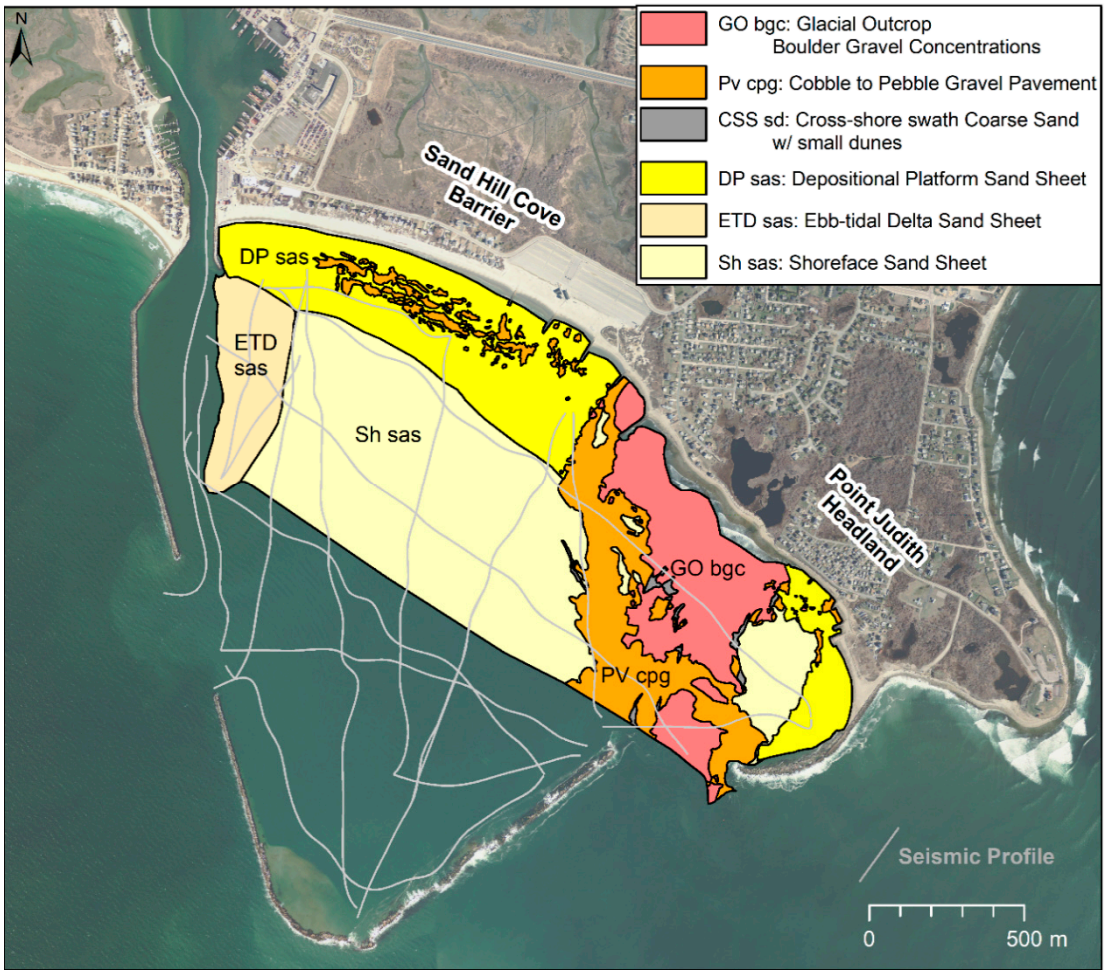


**Figure 2.** Simplified benthic geologic habitats of the upper shoreface within the HoR. Extent of the units was interpreted from side-scan sonar imagery collected in 2015. See Oakley et al. [14] for detailed descriptions of the shoreface units.

## 3. Materials and Methods

High-resolution geophysical profiles, bathymetry mapping, and sediment cores were used to assess and quantify the Point Judith HoR sediment budget following construction of the three main breakwaters. The thickness and volume of post-construction sediment interpreted from seismic profiles were compared to changes in bathymetry from historic hydrographic data. Sedimentation rates were calculated using lead-210 isotopes.

### 3.1. Sub-Bottom Data and Analysis

Subsurface interpretations are based on 28 km of sub-bottom seismic reflection profiles (Figure 1) collected in 2016, using an EdgeTech (Wareham, MA, USA), SB-216S Full-Spectrum sub-bottom profiler (frequency sweep 10 kHz). Towfish height was maintained at 1 m below the water surface, towed at < 6.5 km·s$^{-1}$. Spatial location was embedded into sub-bottom files using the serial output of a Trimble DSM-132 GPS with a reported accuracy of ±1 m. An additional 6 km of profiles were collected in 2017 using a Teledyne Benthos (North Falmouth, MA, USA) CHIRP III sub-bottom profiler (2–7 kHz frequency sweep) powered by a Teledyne Benthos DSP-664 transceiver. The assumed vertical resolution the seismic reflection methods was <15 cm. Profiles were post-processed using Chesapeake Technologies (Mountain View, CA, USA) Sonar Wiz v.6. Processing of seismic profiles was used to adjust for differences in gain and contrast prior to interpretation, and some profiles required a swell filter to remove motion imparted by waves. Depth to reflectors was calculated using an acoustic velocity of 1500 m·s$^{-1}$. Sonar records were not tide-corrected, which has no effect on the relative measurement (thickness of the sediment between digitized reflectors).

### 3.2. Sub-Bottom Seismic Reflection Interpretation

Sediment thickness was determined by manually digitizing the seafloor and underlying reflectors using using Chesapeake Technologies (Mountain View, CA, USA) SonarWiz Software v. 6 and was calculated as the difference in relative elevation between the two surfaces. An isopach grid was interpolated using the natural neighbor algorithm within the ESRI (Redlands, CA, USA) ArcGIS v. 10.3 Spatial Analyst. The pixel size for the resulting grids was set at 5 m, similar to the reported accuracy of the Differential Global Positioning System (DGPS) utilized for the sub-bottom profiles (1–3 m). The resulting grid was then clipped using the mapped extent of the seismic reflection profiles. Volume calculations were performed using the Functional Surface tool within the three-dimensional (3D) Analyst extension of ESRI ArcMap v. 10.3. Uncertainty estimates are based on the areal extent of the interpolation multiplied by an uncertainty factor. The vertical uncertainty factor of 0.25 m is based on the estimated digitization error (0.1 m) and the minimum resolution of the sub-bottom profiles (0.15 m) [37,38]. This value likely represents a conservative error estimate.

### 3.3. Bathymetric Data and Analysis

Historic hydrographic soundings, surveyed in 1904 [21] and 1913 [22] using lead lines were digitized and compared to digital soundings ($n$ = 6274) from a 2009 NOAA bathymetric survey [39]. Uncertainty of the bathymetric data was not assessed; however, the 2009 survey would have a maximum uncertainty of 1.3% of the water depth (0.13 m for 10 m water depth) [40]. Uncertainty of the lead line surveys, particularly the positional accuracy, is difficult to assess. The vertical measurement of a lead line survey is likely within 0.07 m, with a total uncertainty (encompassing water level corrections and interpolation) closer to 0.5 m [41,42]. The two hydrographic sheets were georeferenced in ESRI (Redlands, CA, USA) ArcMap using 2014 U.S. Geological Survey Digital Orthophotos [43]. Resulting horizontal uncertainties, expressed as the root mean square of the error, was less than 15 m for both the 1904 and 1913 maps. Soundings from the lead line surveys were manually digitized as points (1904: $n$ = 2304; 1913: $n$ = 2171). The reported values were corrected for the difference in elevation between the datum used in 1904/1913 surveys (mean low water) and the 2009 survey datum (mean

lower low water (MLLW)) as reported for the Newport, RI tide gauge (25 km northeast of the HoR; +0.11 m). Tidal range and data along the RISS are comparable to the Newport Tide gauge [44]. Depths were also corrected for sea level rise (2.72 mm·year$^{-1}$), using the measured (1929–2017) rate of rise at the Newport Tide Gauge [45]. These adjustments increase the 1904 soundings by 0.39 m and the 1913 soundings by 0.37 m. The preferred approach would be to find the historical benchmarks and resurvey them to determine the elevation relative to a modern datum [46,47]; however, the benchmarks installed during the 1904 and 1913 surveys could not be relocated. Given the relatively low tidal range (great diurnal range 1.03 m (3.85 ft) [17], the method used here provides a good first approximation of the vertical offsets. However, the total vertical uncertainty cannot be calculated for the adjusted soundings. Continuous surfaces were interpolated from the digitized soundings using the natural neighbor algorithm. The pixel size for the resulting grids was set at 5 m. Subtracting the historic surfaces from the 2009 surface using the ESRI ArcMap raster calculator produced continuous surfaces representing the change in elevation between surveys. The volume of eroded (negative values) and deposited (positive values) sediment was calculated using the Functional Surface tool within the 3D Analyst extension of ESRI ArcMap v. 10.3.

### 3.4. Sediment Coring

Sediment cores were collected using a Rossfelder (Poway, CA, USA) P-3 Vibro-Percussive system, accommodating 7.6 cm diameter, 3 m long steel core barrels with plastic core liners. The location, water depth, time, and measurements of cable tension were documented during coring at each station. The core barrel assembly was removed from the vibracore head following recovery, and the core liner was extruded from the barrel. The recovered sediment length was measured, and the core was packaged for storage. For isotope analysis of sedimentation rates, two additional cores were recovered using a 10.2 cm polycarbonate piston corer, which maintains the sediment–water interface allowing for more accurate downcore measurements. All cores were kept refrigerated and subsequently imaged on a GEOTEK multisensory track data core logging system. Grainsize was measured using a Malvern Panalytical (Westborough, MA, USA) Mastersizer 2000 laser diffraction particle size analyzer, which measures 101 grainsize bins between 0.01 µm and 1000 µm (1 mm). Grainsize analysis was conducted on samples at 5 cm intervals downcore. The piston cores were subsampled every 5 cm (0 between 60 cm) and at 10 cm intervals from 60 cm to the base of cores and analyzed for nuclides of $^{210}$Pb and $^{137}$Cs. The second half of the core was archived in refrigerated storage.

### 3.5. Isotope Analysis

Sedimentation rates were obtained by analyzing core samples for $^{210}$Pb and $^{137}$Cs radioisotopes using gamma spectroscopy. Dried and homogenized samples were packed in Petri dishes and sealed with electrical tape and paraffin wax 30 days prior to analysis to allow for equilibration between $^{226}$Ra and its daughter isotopes, $^{214}$Pb and $^{214}$Bi (supported $^{210}$Pb). Total $^{210}$Pb (46.5 keV photopeak) and $^{137}$Cs (662 keV photopeak) activity was measured for all samples along each core using a Canberra GL 2020 low-energy germanium detector at the Virginia Institute of Marine Science Geochronology Lab. Total $^{210}$Pb counts were corrected for detector efficiency and self-attenuation using the point-source method [48]. Concentrations of excess $^{210}$Pb used to obtain age models were determined as the difference between total and supported $^{210}$Pb. $^{137}$Cs is a bomb-produced radionuclide used to verify accumulation rates determined by $^{210}$Pb geochronology. Peak $^{137}$Cs activity is assumed to be 1963. The constant flux-constant sedimentation (CFCS) model [49] was used to calculate sedimentation rates over the past ~100 years for both cores. The constant rate of supply (CRS) model [49,50] was applied to core HoR-3B to calculate age of individual samples down core; due to sampling errors where bulk density could not be accurately determined, this model was not applied to core HoR-1B.

## 4. Results

### 4.1. Sub-Bottom Seismic Reflection Profiles

Sub-bottom profiles collected within the HoR (Figure 1) showed a distinct seismic facies configuration, with a continuous, underlying regional seismic reflector, overlain by largely acoustically transparent sediment from 0 to > 4 m thick. The underlying reflector is relatively flat with a seaward slope, although hummocks and swales interpreted as boulder to cobble gravel topographic highs occur in places. The tops of the hummocks are overlain by a thin layer of acoustically transparent sediment. Figures 3–6 are seismic reflection profiles showing the thickness and distribution of sediment above the ravinement surface. Figure 7 shows the interpolated post-construction sediment thickness. Sediment deposited above this surface is confined to the western and central portions of the HoR and is between 1 and 2 m thick (Figure 7). Sediment thickness exceeds 2 m across 18% of the mapped area, and the thickest deposits exceed 4 m at the broad ridge adjacent to the inlet into Point Judith Pond (Figure 4), as well as near the center of the HoR.

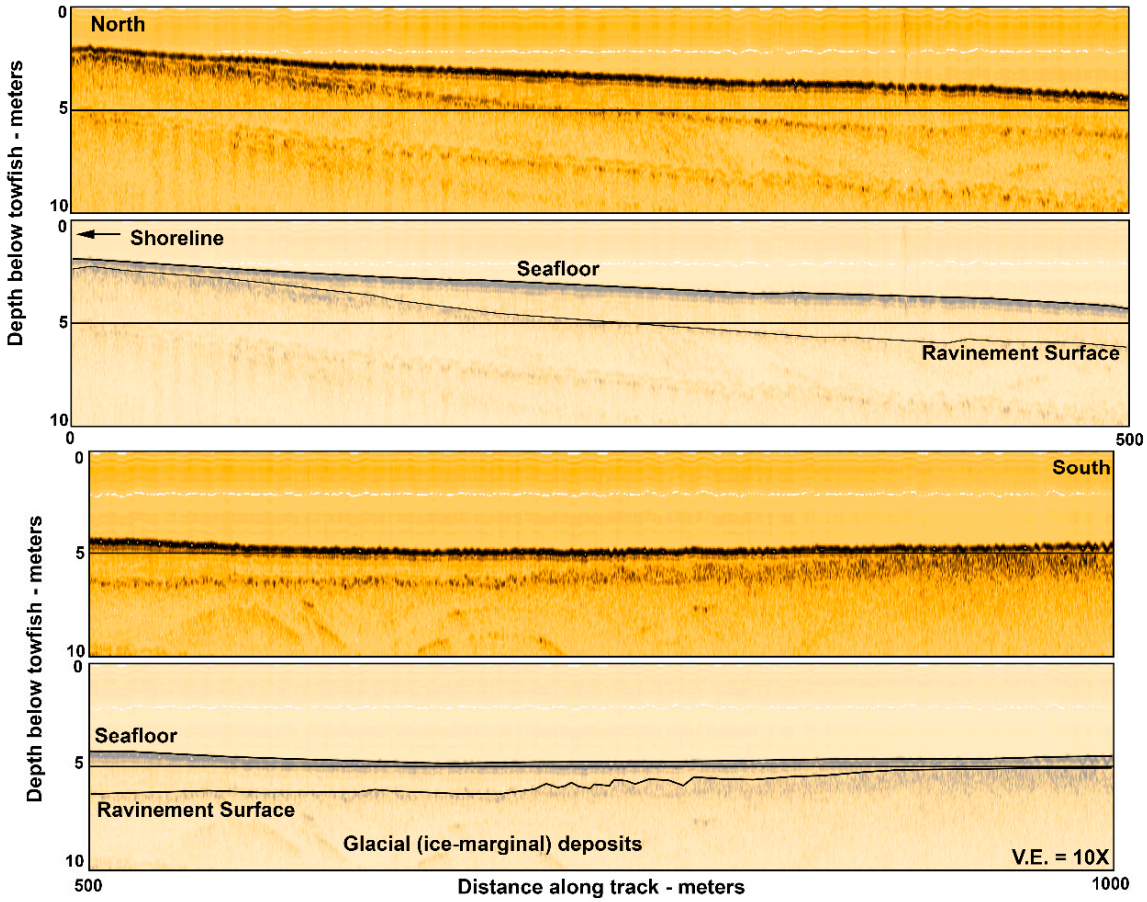


**Figure 3.** Shore perpendicular seismic reflection profile from the northwest corner of the HoR extending from the upper shoreface south toward the center of the harbor, showing the seismic unit overlying the ravinement surface. See Figure 1 for the location of the survey line. Vertical exaggeration is 10× for both profiles; differences in the horizontal scale are due to slight differences in vessel speed during the survey.

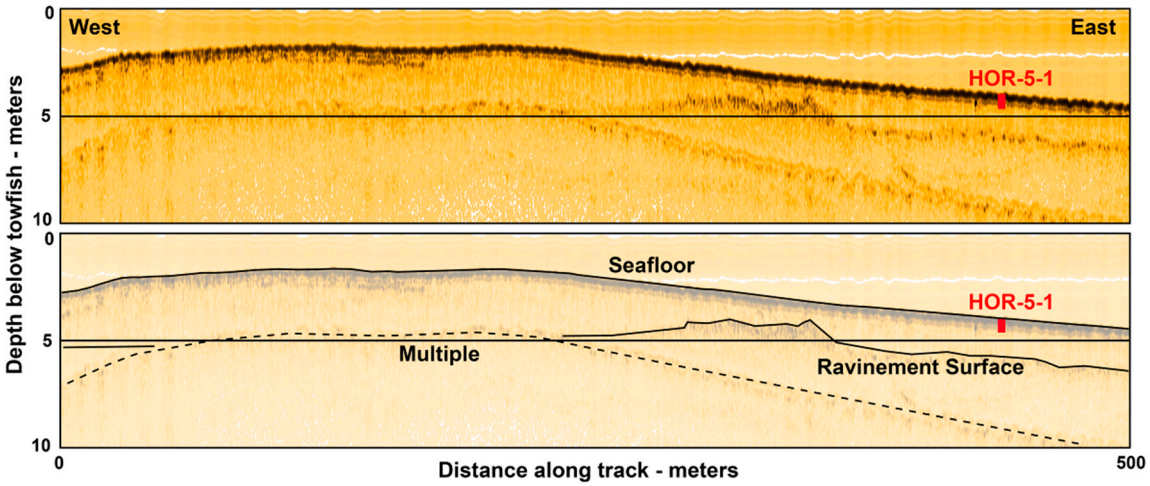


**Figure 4.** Seismic reflection profile from the northwest corner of the HoR running roughly west to east across a portion of the ebb-tidal delta. Red lines show the location of core HoR-5-1. See Figure 1 for the location of the survey line. Vertical exaggeration is 10×.

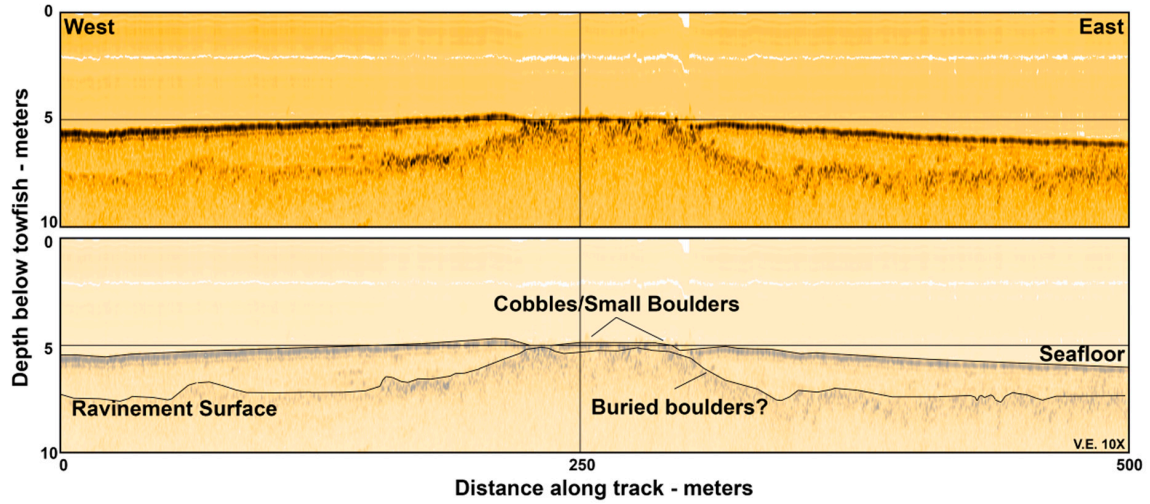


**Figure 5.** West to east trending seismic reflection profile from the center of the HoR extending across the (now buried) topographic high showing the seismic unit overlying the ravinement surface. Note the presence of cobbles/small boulders visible at the surface and possible buried boulders. See Figure 1 for the location of the survey line. Vertical exaggeration is 10×.

Sediment thinner than 1 m covers 26% of the mapped area, largely in the northern and northeastern portions of the HoR, as well as near the western and eastern entrances to the harbor. Other areas with limited sediment deposition are on the shoal extending SSE from the inlet, as well as adjacent to the eastern and western entrances of the harbor (Figure 7). Seismic penetration in the northeastern portion of the HoR was limited by the outcropping gravel pavement, interpreted as an erosional surface following Holocene transgression of coarse-grained glacial deposits. The proximity to the eastern entrance, which is open to southeast storm waves, indicates that this area is nondepositional. Gas-attenuated reflectors were mapped in the southern portion of the HoR (Figure 6) above a reflector approximately 2 m below the seafloor. The source of this gas (typically methane) is likely either recent (Holocene) accumulation and decay of organic sediment or the decay of buried organic rich deposits (i.e., freshwater or salt marsh deposits) [51–53]. Cores HoR-1B and HoR-1, collected near these reflectors did not penetrate deep enough to intersect the gas-attenuated reflectors (Figure 6), and both the source of the gas and the characteristics of the seismic reflector remain unclear.

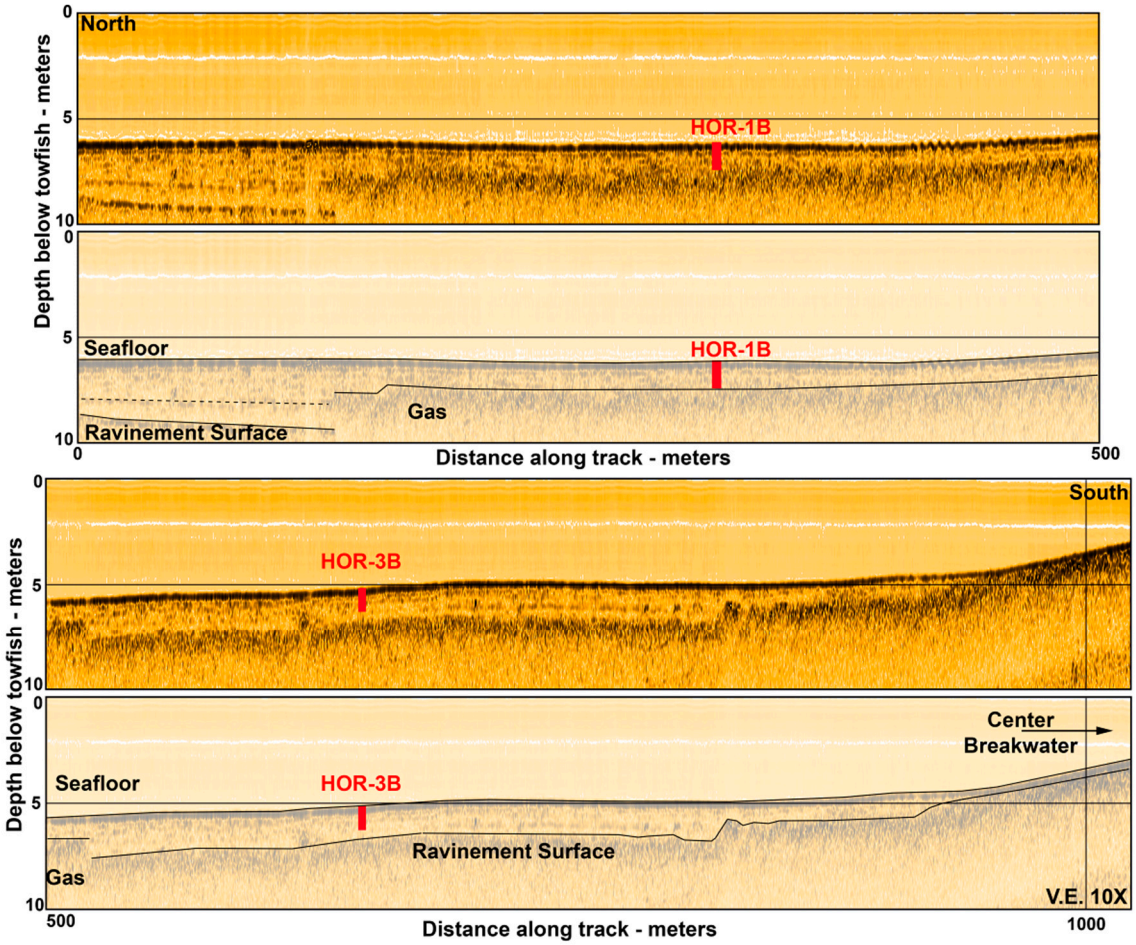


**Figure 6.** North-northeast to south-southwest trending seismic reflection profile showing the seismic unit overlying the ravinement surface. The seismic profile was collected near the apex of the central breakwater. Red lines show the location and depth of sediment cores HoR-1B and HoR-3B. Note that cores HoR-1-1 and HoR-3-4 were collected in similar locations to HoR-1B and HoR 3-B, respectively. See Figure 1 for the location of the survey line. Vertical exaggeration is 10×; differences in the horizontal scale are due to slight differences in vessel speed during the survey.

### *4.2. Bathymetric Surfaces*

Comparison of the surfaces interpolated from the historic bathymetry shows a general pattern of shoaling within the HoR since 1904. Figure 8A–C show the three interpolated surfaces, displayed using the same color ramp. The increase in lighter blue and decrease in purple shades between 1904/1913 and 2009 represents a decrease in water depths over time. The 25 m rectangular feature in the southeast corner of the 2009 survey is a shipwreck [54]. The deepest portion of the HoR is the southeast corner of the survey area and was reported as 11 m below MLLW in 1904 and 10.7 m in 1913 (depths adjusted for sea level rise and tidal datums). The same area in 2009 was >2 m shallower. The arithmetic difference between the 2009 bathymetry and 1904 (Figure 8D) and 1913 (Figure 9E) surveys reveals a similar pattern of shoaling as the seismic profiles (Figure 8F). The total volume of sediment deposited between 1904 and 2009 was $2.8 \times 10^6$ m$^3$. Compared to $2.2 \times 10^6$ m$^3$ between 1913 and 2009 (Table 1). Annualized rates of deposition based on bathymetric changes are similar at $2.7 \times 10^4$ m$^3$·year$^{-1}$ (1904–2009) and $2.3 \times 10^4$ m$^3$·year$^{-1}$ (1913–2009) (Table 1). Comparisons between the historic and 2009 bathymetric surveys suggest that there has been net erosion on the uppermost shoreface following the construction of the breakwaters (Figure 8D,E). The net volume lost was $3.2 \times 10^5$ m$^3$ between 1904 and 2009, with a similar value ($3.4 \times 10^5$ m$^3$) between 1913 and 2009.

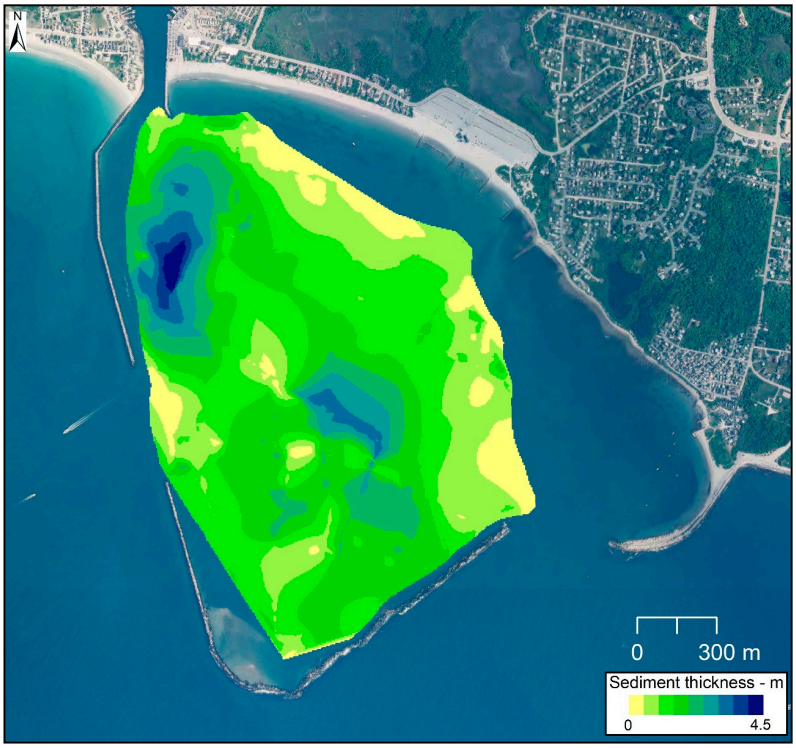


**Figure 7.** Interpolated sediment thickness within the HoR from seismic reflection profiles. The eastern portion of the HoR and shoreface showed no resolvable sediment above the ravinement surface.

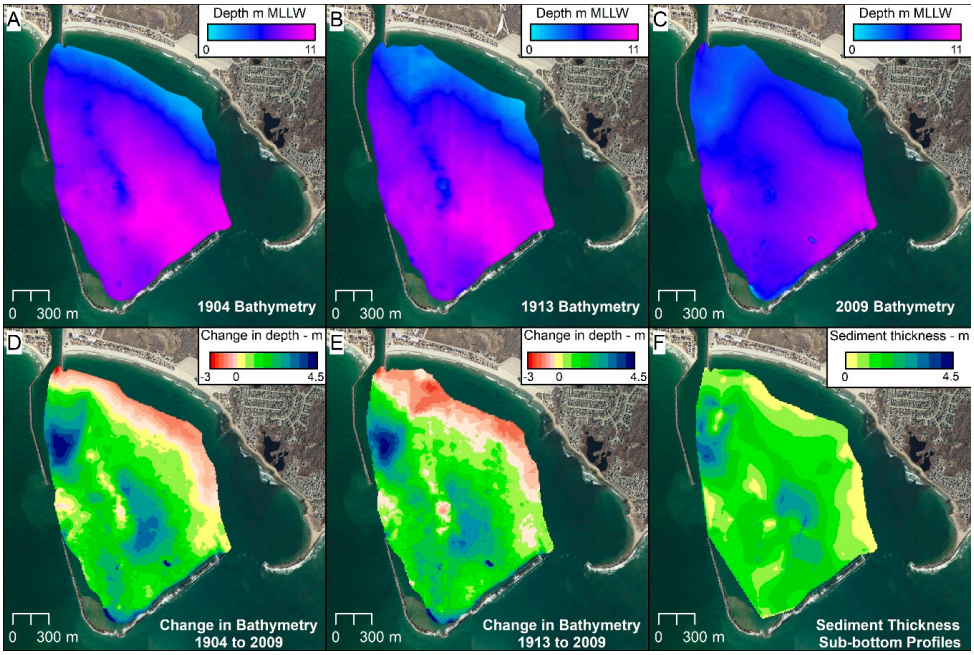


**Figure 8.** (**A**). Bathymetry in 1904 (m below 2009 mean lower low water (MLLW)) (**B**). Bathymetry in 1913 (m below 2009 MLLW) (**C**). Bathymetry in 2009 (m MLLW). Note that all three panels (**A**–**C**) are displayed using the same color ramp, and the shoaling is apparent by the decrease in purple (deeper areas) in 2009 and erosion of the upper shoreface shown by the darker blues in the same period (**D**). Difference in elevation between 1904 and 2009 bathymetric surfaces (**E**). Difference in elevation between 1913 and 2009 bathymetric surfaces (**F**). Sediment thickness interpreted from sub-bottom profiles.

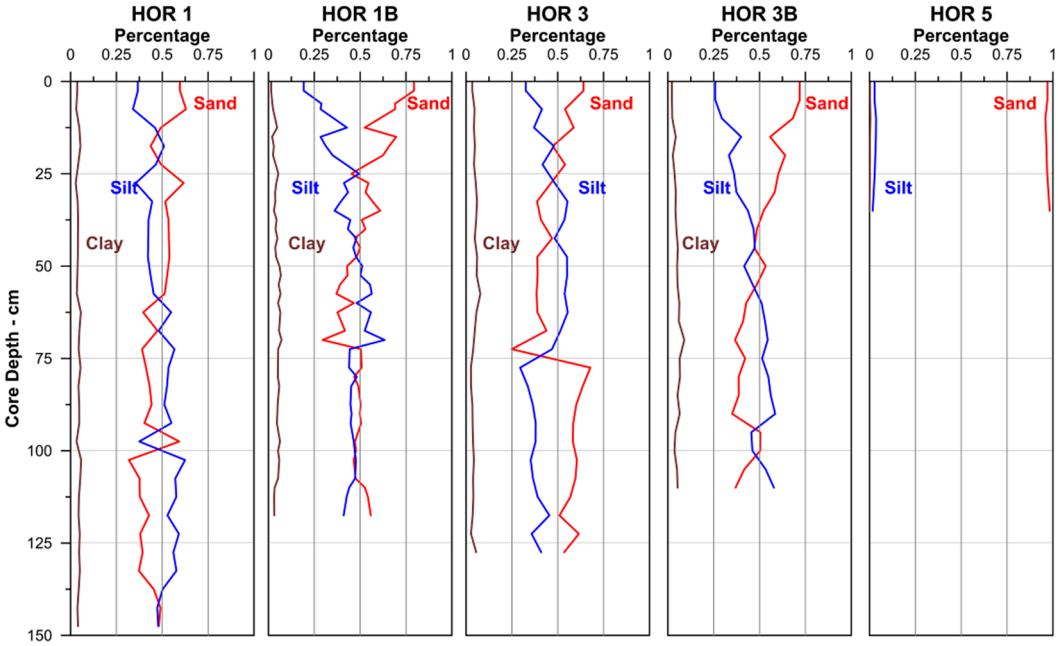


**Figure 9.** Grainsize measured for cores HoR-1, HoR-1B, HoR-3, HoR-3B and HoR-5. Full textural data is available in the supplemental materials.

**Table 1.** Total sediment volume and annualized deposition rate (over 125 years) for the seismic profiles and bathymetric comparisons.

| Method | Time Period | Total Volume ($m^3$) of HoR | Annualized Deposition Rate ($m^3 \cdot year^{-1}$) |
|---|---|---|---|
| Seismic Survey | 1891–2016 | $3.1 \times 10^6$ | $2.5 \times 10^4$ |
| Bathymetric Changes | 1904–2009 | $2.9 \times 10^6$ | $2.8 \times 10^4$ |
| Bathymetric Changes | 1913–2009 | $2.2 \times 10^6$ | $2.3 \times 10^4$ |

### *4.3. Sediment Coring*

Eleven attempts were made to collect vibracores at five locations within the HoR in May 2018. Minimal penetration was achieved and/or no recovery occurred at four locations; five recovered cores were <0.6 m. Two vibracores exceeded 1 m. The results of the coring attempts are summarized in Table 2. Three vibracores (HoR 1-1, HoR 3-4, and HoR 5-1) were selected for grainsize analysis. Two additional cores collected using the polycarbonate piston corer in November 2019 were recovered in the same general locations (HoR-1B (recovered length 1.15 m) and HoR-3B (recovered length 1.2 m)) for isotopic analysis of $^{210}$Pb and $^{137}$Cs. The positions of HoR-1B and HoR-3B are shown in Figure 1; HoR-1-1 and HOR3-4 were collected within 100 m of these locations and are not shown. Sediment texture results of the five cores are shown below. Cores HoR-1, HoR-1B, HoR-3, and HoR-3B demonstrate a general coarsening upward over the upper 0.25 m, ranging from sandy silt to silty sand on the basis of the Shepard [55] classification system (Figure 9). A surface sediment sample collected 125 m west of core HoR-1B by the US Geological Survey (Sample NBIS70, [56]) (77% sand, 22% silt and 1% clay) is nearly identical to the surface sample of HoR-1B (79% sand, 19% silt, 1.5% clay). The four cores collected in the central basin of the HoR averaged 50% sand (predominately fine to very fine sand), although this varied downcore from 25% to 79% sand. Core HoR-5-1, taken on the shoreface within the northern parts of the HoR, was largely sand. The inlet channel and adjacent ebb-tidal delta is composed of >90% sand [36].

**Table 2.** Summary of core attempts. Core type is abbreviated; VC = vibracore; P = piston core Estimated sediment thickness from seismic reflection profiles.

| Core | Core Type | Latitude | Longitude | Water Depth (m) | Core Length (m) | Interpolated Thickness (m) |
|---|---|---|---|---|---|---|
| HoR 5-1 | VC | 41.36955 | −71.50963 | 5.2 | 0.5 | 1.8 |
| HoR 5-2 | VC | 41.36955 | −71.50963 | 5.2 | 0.5 | 1.8 |
| HoR 4-1 | VC | 41.36752 | −71.50090 | 5.0 | 0.0 | 1.3 |
| HoR 4-2 | VC | 41.36752 | −71.50090 | 5.0 | 0.0 | 1.3 |
| HoR 4-3 | VC | 41.36745 | −71.50090 | 5.5 | 0.1 | 1.3 |
| HoR 2-1 | VC | 41.36407 | −71.50153 | 6.7 | 0.6 | 1.4 |
| HoR 1-1 | VC | 41.36095 | −71.50460 | 7.6 | 1.8 | 2.5 |
| HoR 3-1 | VC | 41.35615 | −71.50785 | 5.8 | 0.0 | 0.9 |
| HoR 3-2 | VC | 41.35615 | −71.50785 | 5.8 | 0.3 | 0.9 |
| HoR 3-3 | VC | 41.35620 | −71.50785 | 6.4 | 0.6 | 1.0 |
| HoR 3-4 | VC | 41.35620 | −71.50737 | 6.4 | 1.4 | 1.5 |
| HoR 1B | P | 41.36095 | −71.50460 | 7.7 | 1.2 | 2.4 |
| HoR 3B | P | 41.35620 | −71.50740 | 5.8 | 1.1 | 1.4 |

### 4.4. Lead 210 Isotope Analysis

The CFCS $^{210}$Pb model was applied to the measured concentrations in cores HoR-1B and HoR 3B. Concentrations of excess $^{210}$Pb ranged between 25 and 40 Bq·kg$^{-1}$, except the base of HoR-1B, which decreased to 12.5 Bq·kg$^{-1}$ at 1.2 m (Figure 10). Average accretion rates were calculated as the slope of a best-fit linear regression line of the natural log of excess $^{210}$Pb [49]. The resulting best-fit lines showed relatively poor fits (HoR-1B, 2.3 cm·year$^{-1}$, $R^2$ = 0.25; HoR-3B, 0.78 cm·year$^{-1}$, $R^2$ = 0.02). The poor fit of these lines suggests that the accretion rate varied downcore and makes any age-depth model suspect; however, applying these values places the base of the cores at AD 1967 (HoR-1B) and 1878 (HoR-3B). The $^{137}$CS results are not robust for both cores, given the relatively low concentrations of $^{137}$Cs (< Bq·kg$^{-1}$); however, assuming a small spike in $^{137}$Cs at a depth of 0.4 m in HoR-3B represents the peak of atmospheric testing in AD 1963, the sedimentation rate would be ~0.7 cm·year$^{-1}$, similar to the calculated sedimentation rate. A second peak in $^{137}$Cs at 0.9 m complicates this interpretation and could place the accretion rate as high as 1.6 cm·year$^{-1}$. There is no discernable peak in the $^{137}$Cs measurements observed in HoR-1B. The CRS Accretion Model was applied to HoR 3-B, placing the age at the base of the core at 1917, with an average sedimentation rate 0.57 cm·year$^{-1}$ (accretion rate ranged from 1.10 to 0.06 cm·year$^{-1}$) similar to the CFCS rate of 0.78 cm·year$^{-1}$ (Figure 11).

### 4.5. Total Volume of Post-Construction Sediment

The volume of deposited sediment and the annualized rates are similar between estimates from both the seismic and the historic bathymetric data, and, given the uncertainties in the various methods, the slight differences are likely not substantial. Taken together, the total deposition within the center of the HoR is > 3 × 10$^6$ m$^3$ (Table 1). Outside of the seismic survey area, sediment deposition at the apex of the center wall (visible in orthophotographs (Figure 1)) [25] is estimated to be 4 × 10$^5$ m$^3$ (average thickness of 7 m according to the historic bathymetric surveys). An estimated 1 × 10$^5$ m$^3$ of sediment has also accumulated inside the eastern breakwater and is visible in aerial photographs (Figure 1). Within the HoR, the ebb-tidal delta contains an estimated 7.5 × 10$^5$ m$^3$ of sediment (Figure 12). The flood-tidal delta represents an additional 1.4 × 10$^6$ m$^3$ according to the annualized rates of deposition [31]. Taken together, these estimates suggest a total sediment volume within the HoR and adjacent Point Judith Pond to be 5.0 × 10$^6$ m$^3$. Sediment cores and sediment grab samples ranged from 30% to >90% sand within the central basin. The ebb-tidal delta, as well as the sediment at the apex of the central breakwater and inside the east breakwater, is assumed to be >90% sand. Table 3 summarizes the total sediment volume and estimated sand volume for the deposition sinks within

the HoR. The total sand volume reported here ($3.6 \times 10^6$ $m^3$; annualized rate of deposition $2.9 \times 10^4$ $m^3 \cdot year^{-1}$) is likely a conservative estimate.

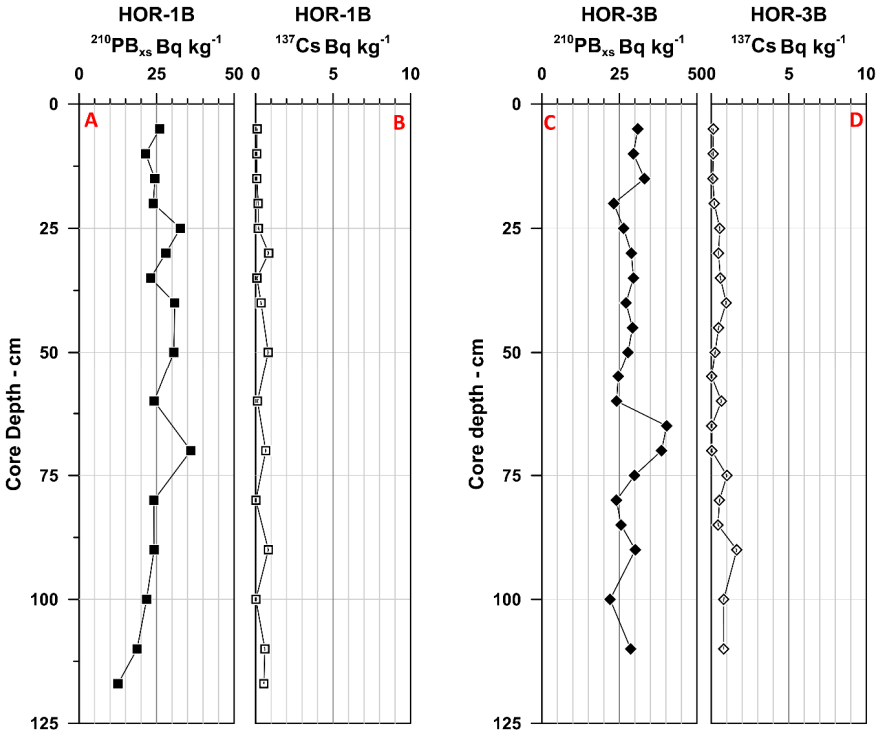


**Figure 10.** Constant flux-constant sedimentation (CFCS) model showing (**A**) excess $^{210}$Pb and (**B**) total $^{137}$Cs (Bq·kg$^{-1}$) for core HoR-1B, as well as (**C**) excess $^{210}$Pb and (**D**) total $^{137}$Cs (Bq·kg$^{-1}$) for core HoR-3B. See core location in Figure 1. The full results of the analysis are available in (Table S6 Supplementary Materials).

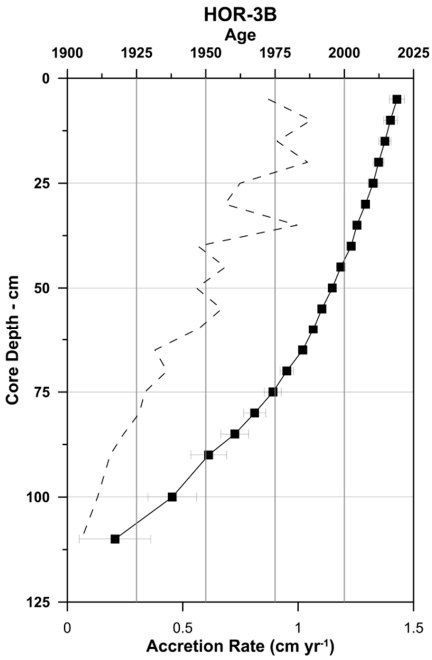


**Figure 11.** Sediment age dates (solid line) and accumulation rate (dashed line) calculated using the constant rate of supply (CRS) model. See Figure 1 for the location of the core. The full results of the analysis are available in (Table S7 Supplementary Materials).

**Table 3.** Total volume, percentage sand, and estimated sand volume of the depositional sinks within the HoR (* grainsize ranges from 30% to >80% sand; 50% likely represents a conservative estimate).

| Depositional Sink | Total Volume ($m^3$) | Percent Sand | Sand Volume ($m^3$) | Source |
|---|---|---|---|---|
| Central basin | $2.3 \times 10^6$ | * 50% | $1.2 \times 10^6$ | Seismic/bathymetry |
| Ebb-tidal delta | $7.5 \times 10^5$ | >90% | $6.8 \times 10^5$ | Seismic/bathymetry |
| Flood-tidal delta | $1.4 \times 10^6$ | >90% | $1.3 \times 10^6$ | Boothroyd et al., 1985 |
| Eastern breakwater | $1.0 \times 10^5$ | >90% | $0.9 \times 10^5$ | Estimated from bathymetry |
| Center axis | $4.0 \times 10^5$ | >90% | $3.6\times 10^5$ | Estimated from bathymetry |
| Total Volume | $5.0 \times 10^6$ | | $3.6 \times 10^6$ | |
| Annualized Rate | $4 \times 10^4$ $m^3 \cdot year^{-1}$ | | $2.9 \times 10^4$ $m^3 \cdot year^{-1}$ | |

## 5. Discussion

Deposition within a breakwater harbor is fairly common, due to reduced incident wave energy and interruption of longshore sediment transport [57]. The onset of sediment deposition was likely coincident with the emplacement of the structures, as rapid infilling is common when there is an adequate sediment supply [2,57–64]. The volume of sediment here is noteworthy, however, given the sediment starved nature of the RISS ([13,14]. Sediment sinks are confined to three main areas within the HoR, the central basin, flood-tidal delta, and ebb-tidal delta. Smaller deposits were also identified inside the eastern breakwater and at the apex of the central breakwater. Table 3 summarizes the total sediment volume within these sinks. Deposition in the center of the HoR occurs to the east of the roughly north to south trending bathymetric high seen in the 1904 and 1913 surveys (Figure 8). The relatively complicated pattern of deposition shown in Figures 3–6 suggests that, rather than a simple basin fill model, deposition occurred on top of and around a complex shoreface topography. Given the glacial inheritance of the region, a heterogeneous shoreface is expected [14], with cobble to boulder gravel occurring throughout the study area. Figures 5 and 8A,B show a good example of cobble to boulder gravel topographic highs on the shoreface. The hummocky topography of the ravinement surface has been largely buried, particularly in the western and central portion of the HoR. Whereas the antecedent topography controls the properties of the shoreface [65–67], it appears that the deposition of sediment following breakwater construction has covered and buried some of the original shoreface topography. Elsewhere along the RISS, the upper shoreface offshore of the barriers and headlands is dominated by the shoreface depositional platform, a deposit of sand >2 m thick overlying the ravinement surface, extending offshore to a water depth of 7–8 m [14]. The upper shoreface seaward of the depositional platform is a mixture of cobble-gravel pavement and coarse sand, mapped as a thin reworked layer over the underlying glacial deposits [14]. Whereas ebb-tidal deltas are absent along the open coast of the RISS, as is typical for sediment starved, microtidal, wave-dominated coastlines [18], the accumulation of sediment adjacent to the inlet into Point Judith Pond represents the terminal lobe/channel margin linear bar of a complicated ebb-tidal delta complex [68], which has formed within the HoR due to reduced wave energy. This landform accounts for 25% of the total volume deposited ($7.5 \times 10^5$ $m^3$); according to sediment samples, the ebb-tidal delta is composed of >90% sand (>$6.8 \times 10^5$ $m^3$).

The erosion of the uppermost shoreface within the HoR over the last century of >$3.0 \times 10^5$ $m^3$ (Figure 8D,E) is supported by the apparent lack of sediment accumulation on the uppermost shoreface in seismic records (Figure 3) and the prevalence of cobble gravel cropping out from the underlying glacial deposits (Figure 1), as observed in side-scan sonar records, aerial imagery, and sediment grab samples. This shoreface erosion and the subsequent redistribution of sediment within the HoR accounts for 2% of the sediment deposited within the entirety of the HoR system, suggesting that much of the sediment originated from outside the harbor. Some of the eroded shoreface sediment was likely transported eastward via longshore transport to the inside of the eastern jetty (Figure 12), where $1.0 \times 10^5$ $m^3$ of sediment has accumulated. Transport along the eastern breakwater and out of

the HoR remains uncertain, but the boulder/cobble shoreline east of the HoR suggests that this process is likely not a significant transport pathway for sand. Deposition of sediment within the apex of the central breakwater [25] is another sink of approximately $4.0 \times 10^5$ m$^3$ of sediment.

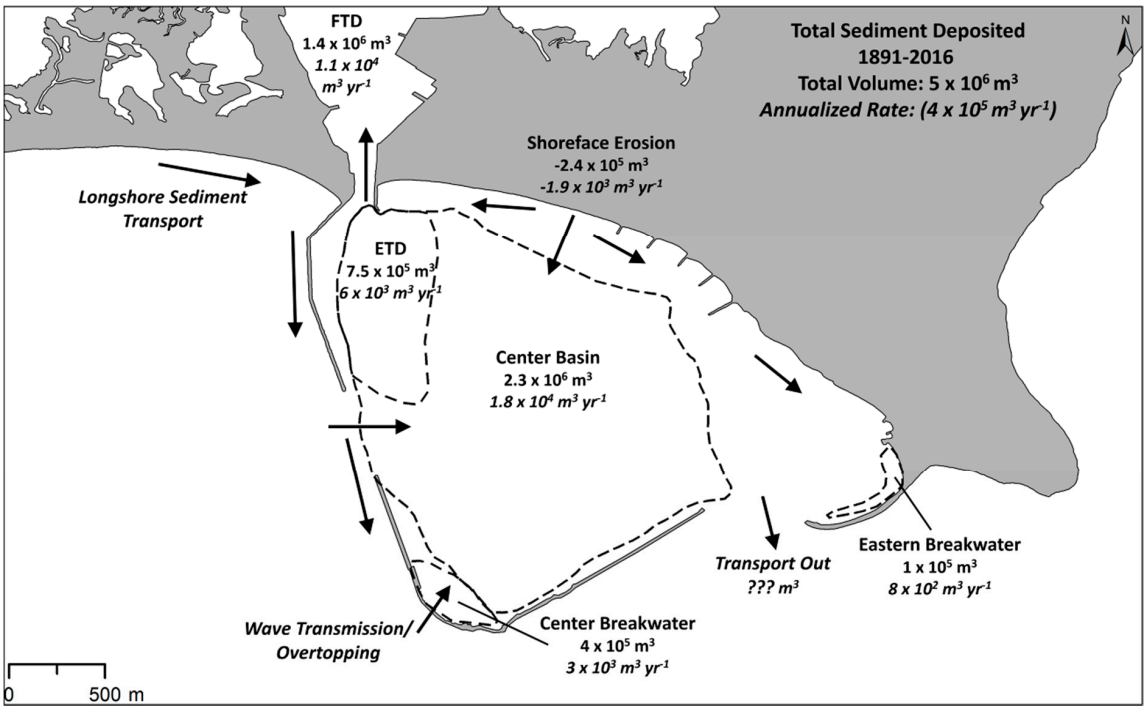


**Figure 12.** Semi-conceptual sediment budget for the Point Judith Harbor of Refuge. Total deposition between 1891 and 2016 and inferred minimum longshore sediment transport from the adjacent RISS. Flood-tidal delta deposition [31]. The wave transmission/overtopping deposition at the apex of the center wall is based on [25]. Other possible pathways are discussed in the text.

Given the likely underestimation at locations, including accumulation within the beaches/dunes and transport from Point Judith Pond into the connected coastal lagoon (Potters Pond), the total deposition within the HoR and adjacent coastal lagoon exceeds $5.0 \times 10^6$ m$^3$ over the previous 125 years (annualized rate $3.9 \times 10^4$ m$^3$·year$^{-1}$). The deposition of $>5.0 \times 10^6$ m$^3$ represents a significant and previously unquantified sediment sink for this system. The annualized rates of deposition of sand-sized sediment within the HoR ($2.9 \times 10^4$ m$^3$·year$^{-1}$) is roughly double the reported sum of annual deposition ($1.5 \times 10^4$ m$^3$·year$^{-1}$) within the other three coastal lagoons along the Rhode Island South Shore with jettied inlets [31]. The likely source for the bulk of the sand-sized sediment deposition within the HoR is longshore sediment transport from the adjacent RISS, entering the HoR via the western entrance (Figure 1). Different rates and directions of longshore sediment transport have been reported along the RISS [69], whereby both Boothroyd [31] and Fisher [70] suggested a net easterly sediment transport. McMaster [71] suggested a more complicated pattern of transport along the RISS, with net transport toward the east into the HoR from the adjacent barrier and headland only. Oakley et al. [14] reported the thickest shoreface deposits on the western side of headlands and adjacent to the western breakwater of the HoR, as well as along other points along the RISS, which also supports net easterly longshore sediment transport along the RISS. The volume of sediment deposited within the harbor over the past 125 years is >4-fold larger than the berm volume for the entire 33 km RISS [13] and is approximately equal to the berm volume combined with the upper shoreface deposits along the entire RISS [14]. This high value suggests that sediment is likely contributed from the entire RISS, although further work is needed to examine the overall sediment budget of the RISS, particularly the contribution of sediment from dune/headland erosion and shoreface erosion/incision into underlying glacial deposits. The total longshore sediment flux along the RISS has not been quantified, but estimate rates have ranged from

$5 \times 10^3$–$3 \times 10^4$ $m^3 \cdot year^{-1}$ [72,73]. The annualized rates of deposition of sand-sized sediment within the HoR reported here suggest that these may represent an underestimation, and further work is needed to better quantify these values.

The source of the finer-grained (silt and clay) sediment is likely a combination of erosion of the glacial headlands (composed of a mixture of till (diamict) and stratified glacial fluvial deposits capped by the eolian mantle composed of silt and very fine sand [26–28] coupled with primary production of organic material and macroalgae and phytoplankton [74]. Shoreface incision into underlying glacial lakefloor deposits and coastal lagoon deposits uncovered during transgression cannot be ruled out as additional sources of sediment. The inlet channel, portions of the ebb-tidal delta and flood-tidal delta are dredged periodically to maintain navigation to the port of Galilee within Point Judith Pond. This sediment, which is composed of >90% sand, is placed on the shoreface 5 km west of the HoR [75]. While the central basin of the HoR contains abundant sediment, it exceeds the typical 10% maximum "fines" for beach replenishment borrow sites [2]. Sediment sources containing >10% silt and clay have increased costs, as well as environmental concerns, as more turbidity is created at the source and during placement [2]. While not currently suitable for beach replenishment, as competition for available sand resources increases, alternative sources may become viable for future projects [2]. More detailed coring studies in the future may show some areas within the HoR may meet the 10% maximum for fine-grained sediment, particularly closer to the shoreface and ebb-tidal delta. Prior to construction of the breakwaters, sediment likely bypassed Point Judith. McMaster [71] suggested that longshore transport to the north from Point Judith was responsible for the deposition of sandy sediment along the east facing shoreline between Narragansett Bay and Point Judith, and some of this sediment was likely transported from the RISS. The volume of sediment transported today from the HoR, out through the eastern entrance and around Point Judith, today remains unclear. The predicted currents within the inlet show some ebb-asymmetry, whereas the cobble to boulder gravel adjacent to the entrance and the preponderance of gravel along the shoreline east of the HoR suggest that this process is not a significant sediment transport pathway for sand.

The accretion rates estimated from radiometric nuclides (0.57 to >2 $cm \cdot year^{-1}$) are consistent with the measured thickness of the sediment above the ravinement surface in seismic reflection profiles. The average thickness (1.5 m) annualized over 125 years yields a rate of 1.2 $cm \cdot year^{-1}$. Seismic profiles near HoR-3B suggest a maximum sediment thickness of 1.4 m, suggesting that the cores reached near the ravinement surface at HoR-3B. This matches the interpreted age of the core base (1917) (Figure 11) and supports the hypothesis that sedimentation began shortly after breakwater construction. Seismic profiles near core HoR-1B suggest the ravinement surface is 2.4 m below the seafloor; however, only 1.2 m of sediment was recovered in the piston core (1.8 was recovered using a vibracore, but isotopes were not analyzed). According to the seismic survey, the sediment thickness of 2.4 m equates to an annualized accretion rate of 1.9 $cm \cdot year^{-1}$, which is comparable to estimated rate based on isotopic analysis (2.3 $cm \cdot year^{-1}$). The CFCS accretion rate at HoR-1B places the age of the core base at AD 1966, with an estimated age of AD 1915 for sediment 2.4 m below the seafloor. It remains unclear if the increased accretion rate in HOR-3B (Figure 11) is related to dredging of the inlet channel in the second half of the 20th century. Taken together, the results of the isotopic analysis support the hypothesis that the sediment within the HoR above the mapped ravinement surface was deposited after the construction of the breakwaters

The total post-construction volume of sediment here is consistent with deposition in other breakwater harbors, although the volume of sediment deposited varies with the size of the harbor and availability of sediment. The Channel Island Harbor breakwater traps approximately $1 \times 10^6$ $m^3 \cdot year^{-1}$, most of the calculated annual longshore transport volume [76]. Similarly, Santa Barbra Harbor, California, which is 10% of the size of the HoR, is dredged annually with an average volume of $2.6 \times 10^5$ $m^3 \cdot year^{-1}$; however, the sediment input to that coastal system (>$2.8 \times 10^6$ $m^3 \cdot year^{-1}$) [77] is greater than the berm volume for the entire RISS [13], suggesting that it is a comparatively sediment-rich coastal system. Other harbors along the California have smaller sediment inputs. Dana Point, California,

a small (0.75 km$^2$) breakwater harbor, has an average sediment input of 4–5 × 10$^3$ m$^3$·year$^{-1}$ [78], ~10% the volume deposited in the HoR. The total sediment budget here is lower, however, with a total input of 27,000 m$^3$·year$^{-1}$ over the entire 13 mile coastal segment [77]. Studies conducted on Breakwater Harbor, located landward of Cape Henlopen Spit, Delaware, reported shoaling rates of 0.6 to 5.7 cm·year$^{-1}$, predominately composed of finer-grained (silt- and clay-sized) sediment [79–81]. These values are similar to, albeit slightly higher than, the rates measured here (1–>3 cm·year$^{-1}$). Pozm Port, Iran, a partially enclosed harbor on the Gulf of Oman, showed a similar volume of deposition to the HoR (43,000 m$^3$·year$^{-1}$) [64]. Point Sapin, New Brunswick, Canada, a small breakwater enclosed harbor (0.04 km$^2$), requires dredging of up to 3 × 10$^4$ m$^3$·year$^{-1}$, similar to the estimated deposition within the HoR; however, the actual volume accumulating is likely higher [73,74]. The variation within these harbors is likely related to a variety of factors, but an underlying factor in all is the availability of sediment within the coastal system entering the harbor via longshore transport, where harbors located along shorelines with high rates of sediment supply annual deposition up to an order of magnitude larger than the HoR.

While the discussions herein are largely empirical, several inferences on sediment transport within the HoR can be discussed. A conceptual sediment budget shown in Figure 12 outlines inferred volumes of sediment deposited since construction of the breakwaters, as well as the potential transport pathways. The distribution of sediment within the western and central portion of the HoR, coupled with previous estimates of longshore sediment transport for the RISS, indicates that most of the sediment entering the HoR comes in via the western entrance, transported from the adjacent RISS. Once inside the breakwaters, a combination of waves, wave-induced currents, and tidal currents disperse the sediment. Waves, likely from the southwest (fair-weather wind direction) transport sediment into the center of the harbor, over and ultimately in the lee of the north to south trending shoal visible in the historic bathymetric surveys (Figure 8A,B). Confluence of sediment transport pathways from both the western and the eastern entrances could also help to focus sediment into a thicker deposit near the center of the HoR. Sediment transport via tidal currents from the HoR into the adjacent lagoon is apparent from both the growth of flood-tidal deltas [31] and the need to dredge the inlet channel and portions of the ebb-tidal delta to maintain navigation. Wave transmission and overtopping could represent a possible process to deposit sediment within the apex of the central breakwater [25]; however, the source of the sediment here remains unclear. Several possibilities exist. For example, the sediment could be transported onshore from the adjacent shoreface [82] and then through/over the central breakwater. Alternatively, sediment could be transported from the adjacent RISS, along the western breakwater, bypassing the entrance and moving along the outside of the breakwater before being transported through/over the central breakwater. Conversely, rather than being transported from the south, this deposit could represent sediment transported along the inside of the breakwater as waves diffract and deposited at the apex of the V-shaped breakwater at the confluence of northwest and northeast wind waves.

The breakwaters limit the fetch within the harbor and produce a complicated longshore sediment transport pattern. Sediment accumulating in the far-eastern end of the harbor suggests that some longshore transport is toward the east driven by prevailing southwest winds during fair-weather conditions. The likely source of sediment is erosion of the shoreline and uppermost shoreface of the Sand Hill Cove Barrier, as the Point Judith headland is mostly composed of diamict with abundant boulders. The groin field in the center of the HoR shows no clear pattern of deposition, with slight accretion on both the east and west sides [33,34], suggesting that transport here may be bimodal. Bimodal transport can be supported, as the largest waves entering the east and west entrances converge on this area, anecdotally observed as a popular surf break during storms. Storm waves from the southeast entering the HoR via the eastern entrance likely drive transport toward the west along the Sand Hill Cove Barrier, supported by the deposition of sediment against the jetty at the eastern side of the inlet, the net accretion between 1939 and 1963, and the relatively low rates of erosion since 1963 [33]. Comparing the modern and historic bathymetric surfaces suggests that the upper shoreface within

the HoR has deepened by >2 m in some areas (Figure 8C,D). Where this sediment was transported (alongshore toward the east, into the adjacent inlet or offshore into the center of the HoR during storms) remains unclear and likely represents a combination of morphodynamic factors.

The erosion of the shoreface over the past century and the lack of sediment deposition on the uppermost shoreface are likely the result of asymmetric cross-shore sediment transport; storm waves entering the harbor can induce both alongshore and offshore sediment transport. The subsequent fair-weather waves are fetch limited by the western and central breakwaters, limiting the onshore transport of sand reported on open coastlines [82,83]. The calculated return depth, where sediment could be returned to the shoreline during a period of fair weather, for the open coast of the RISS, is 12 m [84]. The return depth is different than the depth of closure, which was calculated using hindcast wind data along the RISS and varies from 7 to 9 m depending on the calculation methods [85–87]. The reduction of wave energy during both storm and fair-weather conditions would substantially decrease the return depth within the harbor, thereby altering the depositional processes. Similar observations have been made for the Connecticut Long Island Sound shoreline, where Long Island, New York limits fair-weather wave energy [88]. Future work, both observational and modeling, are needed to quantify these empirical sediment transport pathways.

## 6. Conclusions

An integrated database of seismic reflection profiles, historic bathymetric data, and sediment cores demonstrates that the Point Judith Harbor of Refuge, a breakwater enclosed harbor along the Rhode Island South Shore, is a sediment sink with a total sediment volume of $5 \times 10^6$ $m^3$ deposited above the ravinement surface within the harbor. A comparison of historic and modern bathymetry supports the interpretation that sediment deposition above the ravinement surface within the HoR occurred following the construction of the harbor, which began in 1891. Sediment within the harbor ranges from >90% sand in the inlet channels and tidal deltas to silty sand (average 50% sand) in the center of the harbor. Sediment composition within the central basin of the HoR (30–70% sand) likely limits this deposit as a potential borrow source for beach replenishment. Isotopic $^{210}$Pb analysis on two sediment cores supports the post-construction interpreted formation of the sediment, with vertical accretion rates similar to those estimated from the seismic and bathymetric data. According to seismic reflection profiles, the uppermost shoreface here shows little sediment accumulation on the seismic profiles unlike much of the rest of the RISS. The historic bathymetry shows that the shoreface has eroded over the last 125 years; however, the volume of sediment here is less than 2% of the that deposited within the system, suggesting that the source of much of the sediment is from outside of the HoR. The lack of sediment on the shoreface is likely due to the asymmetric forcing during and following storms. Storm waves can enter the harbor via the eastern entrance and induce offshore sediment transport, whereas the fair-weather waves, predominantly from the southwest, are fetch-limited, reducing onshore sediment transport. The predominant source of sand deposited in the harbor is likely longshore sediment transport from the adjacent RISS, supported by a net easterly longshore transport direction along the RISS, and it suggests that the HoR is a substantial sediment sink and an important component of the RISS sediment budget.

**Supplementary Materials:** The following are available online at http://www.mdpi.com/2077-1312/8/11/863/s1: Table S1 Grainsize data for cores HoR-1-1. Table S2. Grainsize data for core HOR HoR-1B. Table S3, Grainsize data for core HOR3-4. Table S4, Grainsize data for core HoR-3B. Table S5, Grainsize data for core HoR-5-1. Table S6 CIC model data for cores HOR-1B and HOR-3B. Table S7. Isotopic data for core HoR-3B using the CRS model.

**Author Contributions:** Conceptualization, B.A.O. and R.J.H.; methodology, B.A.O.; software, B.A.O.; validation, B.A.O. and C.J.M.; formal analysis, B.A.O., C.J.M., and K.K.L.; investigation, B.A.O., R.J.H., and B.C.; resources, B.A.O.; data curation, B.A.O.; writing—original draft preparation, B.A.O.; writing—review and editing, B.A.O., R.J.H., J.W.K., and B.C.; visualization, B.A.O.; supervision, B.A.O.; project administration, J.W.K. and B.A.O.; funding acquisition, J.W.K. and B.A.O. All authors read and agreed to the published version of the manuscript.

**Funding:** This project was funded by the Department of Interior/National Fish and Wildlife Foundation Hurricane Sandy Coastal Resiliency Competitive Grant Program (grant number 44017), as part of the overall project "Developing Rhode Island's Coastal Resiliency Program", with additional funds from a Connecticut State University American Association of University Professors faculty research grant.

**Acknowledgments:** The authors would like to thank Danielle Cares, Graduate School of Oceanography, University of Rhode Island for assistance with core collection, preparation, splitting and imaging. Danielle Cares and Monique LaFrance assisted with the collection of seismic data in 2017. Chip Heil led the coring effort in 2018; Evan Ernst assisted with core collection in November 2019. The authors would also like to thank Jennifer Connelly (VIMS) for her assistance with the isotopic analysis of the cores and her discussions on $^{210}$Pb isotope ages. The reviewers received from three anonymous reviewers greatly improved the clarity of the final manuscript.

**Conflicts of Interest:** The authors declare no conflict of interest. The funders had no role in the design of the study; in the collection, analyses, or interpretation of data; in the writing of the manuscript, or in the decision to publish the results.

## References

1. Gittman, R.K.; Fodrie, F.J.; Popowich, A.M.; Keller, D.A.; Bruno, J.F.; Currin, C.A.; Peterson, C.H.; Piehler, M.F. Engineering away our natural defenses: An analysis of shoreline hardening in the US. *Front. Ecol. Environ.* **2015**, *13*, 301–307. [CrossRef]
2. USACE. *Coastal Engineering Manual*; U.S. Army Corps of Engineers: Washington, DC, USA, 2006.
3. Pilkey, O.H.; Wright, H.L., III. Seawalls Versus Beaches. *J. Coast. Res.* **1988**, *4*, 41–64.
4. Dean, R.G. Coastal armoring: Effects, principles and mitigation. In Proceedings of the 20th International Conference on Coastal Engineering, Taiwan, 9–14 November 1986; pp. 1843–1857.
5. Dugan, J.E.; Hubbard, D.M.; Rodil, I.F.; Revell, D.L.; Schroeter, S. Ecological effects of coastal armoring on sandy beaches. *Mar. Ecol.* **2008**, *29*, 160–170. [CrossRef]
6. Griggs, G.B. The impacts of coastal armoring. *Shore Beach* **2005**, *73*, 13–22.
7. Church, J.A.; Clark, P.U.; Cazenave, A.; Gregory, J.M.; Jevrejeva, S.; Levermann, A.; Merrifield, M.A.; Milne, G.A.; Nerem, R.S.; Nunn, P.D.; et al. *Sea Level Change*; PM Cambridge University Press: Cambridge, UK; New York, NY, USA, 2013.
8. Emanuel, K.; Sundararajan, R.; Williams, J. Hurricanes and global warming: Results from downscaling IPCC AR4 simulations. *Bull. Am. Meteorol. Soc.* **2008**, *89*, 347–368. [CrossRef]
9. Knutson, T.R.; McBride, J.L.; Chan, J.; Emanuel, K.; Holland, G.; Landsea, C.; Held, I.; Kossin, J.P.; Srivastava, A.K.; Sugi, M. Tropical cyclones and climate change. *Nat. Geosci.* **2010**, *3*, 157–163. [CrossRef]
10. Komar, P.D. The budget of littoral sediments—concepts and applications. *Shore Beach* **1996**, *64*, 18–26.
11. Bowen, A.J.; Inman, D.L. *Budget of Littoral Sand in the Vicinity of Point Arguello, California. Technical Memorandum No. 19*; U.S. Army Coastal Engineering Research Center: Washington, DC, USA, 1966.
12. Rosati, J.D. Concepts in sediment budgets. *J. Coast. Res.* **2005**, *2005*, 307–322. [CrossRef]
13. Boothroyd, J.C.; Galagan, C.W.; Graves, S.M. *Advance and Retreat of the Southern Rhode Island Shoreline, 1939–1985; Including 1985 Berm Volume: Technical Report 7-SRG*; SeaGrant College Program; University of Rhode Island: Narragansett, RI, USA, 1988.
14. Oakley, B.A.; Murphy, C.; Varney, M.; Hollis, R.J. Spatial extent and volume of the shoreface depositional platform on the upper shoreface of the glaciated Rhode Island south shore. *Estuaries Coasts* **2019**. [CrossRef]
15. Rosati, J.D.; Frey, A.H.; Grzegorzewski, A.S.; Maglio, C.K.; Morang, A.; Thomas, R.C. *Conceptual Regional Sediment Budget for USACE North Atlantic Division: Technical Report ERDC/CHLSR-15-2*; Coastal and Hydraulics Laboratory, U.S. Army Engineer Research and Development Center: Vicksburg, MS, USA, 2015.
16. Swift, D.J.P. Coastal erosion and transgressive stratigraphy. *J. Geol.* **1968**, *76*, 444–456. [CrossRef]
17. NOS. Elevations on Station Datum: Point Judith Harbor of Refuge. Available online: https://tidesandcurrents.noaa.gov/datums.html?id=8455083 (accessed on 9 September 2020).
18. Hayes, M.O. Barrier Island Morphology as a Function of Tidal and Wave Regime. In *Barrier Islands from the Gulf of St. Lawrence to the Gulf of Mexico*; Leatherman, S.P., Ed.; Academic Press: New York, NY, USA, 1979; pp. 1–27.
19. Nummedal, D.; Fischer, I.A. Process-response models for depositional shorelines: The German and the Georgia bights. *Coast. Eng. Proc.* **1978**, *1*, 1215–1231.

20. Fitzgerald, D.M.; Van Heteren, S. Classification of paraglacial barrier systems: Coastal New England, USA. *Sedimentology* **1999**, *46*, 1083–1108. [CrossRef]
21. CGS. *H02691: NOS Hydrographic Survey*; Survey, C.A.G., Ed.; Hydrographic Surveys Division, Office of Coast Survey, National Ocean Service, NOAA, U.S. Department of Commerce: Silver Spring, MD, USA, 1904.
22. CGS. *H03521: NOS Hydrographic Survey*; Survey, C.A.G., Ed.; Hydrographic Surveys Division, Office of Coast Survey, National Ocean Service, NOAA, U.S. Department of Commerce: Silver Spring, MD, USA, 1913.
23. Melby, J.A.; Nadal-Caraballo, N.C.; Winkleman, J. *Point Judith, Rhode Island, Breakwater Risk Assessment*, TR-15-13 ed.; Coastal and Hydraulics Laboratory: Vicksburg, MS, USA, 2015.
24. NOAA-NOS. *Datums for 8455083, Point Judith, Harbor of Refuge*; National Ocean Service: Silver Spring, MD, USA, 2004.
25. Lin, L.; Demirbilek, Z. *Coupled BOUSS-2D and CMS-Wave Modeling Approach for Harbor Projects*; U.S. Army Engineer Research and Development Center: Vicksburg, MD, USA, 2012.
26. Boothroyd, J.C.; McCandless, S.J.; Dowling, M.J. *Quaternary Geologic Map of Rhode Island. Interim Map*, 21 Quadrangles ed.; Rhode Island Geological Survey STATEMAP Program: Kingston, RI, USA, 2003.
27. Kaye, C.A. *Surficial Geology of the Kingston Quadrangle: U.S*; Geological Survey Bulletin 1071-1; US Government Printing Office: Washington, DC, USA, 1960; Volume 20.
28. Schafer, J.P. *Surficial Geology of the Narragansett Pier Quadrangle, Rhode Island*; US Geological Survey, Quadrangle Map GQ-140: Washington, DC, USA, 1961.
29. WHG. *Wave, Tide and Current Data Collection, Washington County, Rhode Island: Report to the U.S.*; Army Corps of Engineers by the Woods Hole Group: Bourne, MS, USA, 2012.
30. USACE. *North Atlantic Coast Comprehensive Study: Resilient Adaptation to Increasing Risk: Main Report*; U.S. Army Corps of Engineers: Washington, D.C., WS, USA, 2015.
31. Boothroyd, J.C.; Friedrich, N.E.; McGinn, S.R. Geology of microtidal coastal lagoons: Rhode Island. *Mar. Geol.* **1985**, *63*, 35–76. [CrossRef]
32. NOAA. Current Predictions: Harbor of Refuge, south entrance, Station ID: ACT2266. Available online: https://tidesandcurrents.noaa.gov/noaacurrents/Predictions?id=ACT2266_1 (accessed on 25 September 2020).
33. Boothroyd, J.C.; Hollis, R.J.; Oakley, B.A.; Henderson, R. *Shoreline Change Maps for Washington County Rhode Island Depicting Shoreline Change from 1939–2014*; Rhode Island Geological Survey: Kingston, RI, USA, 2016.
34. Hapke, C.J.; Himmelstoss, E.A.; Kratzmann, M.G.; List, J.H.; Thieler, E.R. *National Assessment of Shoreline Change: Historical Shoreline Change Along the New England and Mid-Atlantic Coasts*; US Geological Survey: Reston, VA, USA, 2010.
35. King, J.W.; Oakley, B.A.; Baxter, C.; Grilli, A.; Spaulding, M.; Fugate, G.; Crean, T.; McCann, J.; Englehart, S.; Meyerson, L.; et al. *An Integrated Program of Environmental Characterization and Monitoring, Modeling, and Engineering to Develop Management Policies and Practices that will Enhance Coastal Resiliency in Rhode Island: FINAL REPORT: Prepared under: National Fish and Wildlife Foundation—Hurricane Sandy Coastal Resiliency Project #2300.14.044017/44017*; The University of Rhode Island: Narragansett, RI, USA, 2019.
36. U.S. Army Corps of Engineers, New England District. *Environmental Assessment for maintenance dredging of the Point Judith Pond Federal Navigation Project, Port of Galilee, Narragansett, Rhode Island*; U.S. Army Corps of Engineers: Concord, MA, USA, 2006.
37. Billy, J.; Robin, N.; Certain, R.; Hein, C.; Berné, S. Barrier shoreline evolution constrained by shoreface sediment reservoir and substrate control: The Miquelon-Langlade Barrier, NW Atlantic. *J. Coast. Res.* **2013**, *2086*, 2089–2094. [CrossRef]
38. Schwab, W.C.; Baldwin, W.E.; Warner, J.C.; List, J.H.; Denny, J.F.; Liste, M.; Safak, I. Change in morphology and modern sediment thickness on the inner continental shelf offshore of Fire Island, New York between 2011 and 2014: Analysis of hurricane impact. *Mar. Geol.* **2017**, *391*, 48–64. [CrossRef]
39. NOAA-NOS. *Hydrographic Survey H12023, Point Judith to Green Hill Point, Project NumberOPR-B363-TJ-09. U.S*; Department of Commerce, N.O.A.A.; National Ocean Survey: Silver Spring, MD, USA, 2012.
40. NOAA. *Field Procedures Manual*; National Oceanic and Atmospheric Administration: Washington, DC, USA, 2014.
41. Saville, T.; Caldwell, J.M. *Accuracy of Hydrographic Surveying in and Near the Surf Zone*; US Beach Erosion Board; U.S. Army Corps of Engineers: Washington, DC, USA, 1953.

42. Byrnes, M.R.; Baker, J.L.; Li, F. *Quantifying Potential Measurement Errors and Uncertainties Associated with Bathymetric Change Analysis (ERDC/CHL CHETN-IV-50)*; US Army Corps of Engineers, Engineer Research and DevelopmentCenter, Coastal and Hydraulics Laboratory: Vicksburg, MS, USA, 2002.
43. RIGIS. *April 2014 Rhode Island Statewide High Resolution Orthoimages*; Rhode Island Geographic Information System (RIGIS) Data Distribution System; Environmental Data Center: Kingston, RI, USA, 2015.
44. Spaulding, M.L.; Grilli, A.; Damon, C.; Fugate, G.; Oakley, B.A.; Isaji, T.; Schambach, L. Application of state of art modeling techniques to predict flooding and waves for an exposed coastal area. *J. Mar. Sci. Eng.* **2017**, *5*, 10. [CrossRef]
45. NOS. Relative Sea Level Trend, 8452660, Newport, RI. Available online: https://tidesandcurrents.noaa.gov/sltrends/sltrends_station.shtml?id=8452660 (accessed on 2 April 2020).
46. Geise, G.S.; Borrelli, M.; Mague, S.T.; Smith, T.L.; Barger, P.; Hughes, P. *Assessment of Multi-Decadal Coastal Change: Provincetown Harbor to Jeremy Point, Wellfleet. A Report Submitted to the Massachusetts Bays Program*; Center for Coastal Studies: Provincetown, MA, USA, 2014.
47. Mague, S.T. Retracing the Past: Recovering 19th century benchmarks to measure shoreline change along the outer shore of Cape Cod, Massachusetts. *Cartogr. Geogr. Inf. Sci.* **2012**, *39*, 30–47. [CrossRef]
48. Cutshall, N.H.; Larsen, I.L.; Olsen, C.R. Direct analysis of 210Pb in sediment samples: Self-absorption corrections. *Nucl. Instrum. Methods Phys. Res.* **1983**, *206*, 309–312. [CrossRef]
49. Corbett, D.R.; Walsh, J.P. 210Lead and 137Cesium. In *Handbook of Sea-Level Research*; Shennan, I., Long, A.J., Horton, B.P., Eds.; Wiley-Blackwell: Hoboken, NJ, USA, 2015; pp. 361–372. [CrossRef]
50. Goldberg, G.D. *Geochronology with 210 Pb*; International Atomic Energy Agency: Vienna, Austria, 1963.
51. Claypool, G.E.; Kvenvolden, K.A. Methane and other hydrocarbon gases in marine sediment. *Annu. Rev. Earth Planet. Sci.* **1983**, *11*, 299–327. [CrossRef]
52. Shubel, J.R. *Gas Bubbles and the Acoustically Impenetrable, or Turbid Character of Some Estuarine Sediments*; Kaplan, I.R., Ed.; Springer: Boston, MA, USA, 1974; Volume 3, pp. 275–298.
53. Ussler, W.; Paull, C.K.; Boucher, J.; Friederich, G.E.; Thomas, D.J. Submarine pockmarks: A case study from Belfast Bay, Maine. *Mar. Geol.* **2003**, *202*, 175–192. [CrossRef]
54. NOAA-NOS. *Point Judith Harbor, NOAA Chart 13219*; National Ocean Service: Silver Spring, MD, USA, 2017.
55. Shepard, F.P. Nomenclature based on sand-silt-clay ratios. *J. Sediment. Res.* **1954**, *24*, 151–158.
56. McMullen, K.Y.; Poppe, L.J.; Ackerman, S.D.; Blackwood, D.S.; Lewit, P.G.; Parker, C.E. *Sea-Floor Geology in Northeastern Block Island Sound, Rhode Island: U.S. Geological Survey Open-File Report 2013–1003*; U.S. Geological Survey: Woods Hole, MA, USA, 2013.
57. Komar, P.D. *Beach Processes and Sedimentation*; Prentice Hall: Upper Saddle River, NJ, USA, 1998.
58. Edwards, B.L.; Namikas, S.L. Changes in Shoreline change trends in response to a detached breakwater field at grand Isle, Louisiana. *J. Coast. Res.* **2011**, *27*, 698–705.
59. Handin, J.W.; Ludwick, J.W. *Accretion of Beach Sand Behind a Detached a Breakwater*; Beach Erosion Control Board Technical Memorandum 16; U.S. Army Corps of Engineers: Washington, DC, USA, 1950; Volume 16.
60. Johnson, J.W. Sand transport by littoral currents. In Proceedings of the 5th Hydraulics Conference, Iowa, IA, USA, 9–11 June 1952; pp. 89–109.
61. King, D.M.; Cooper, N.J.; Morfett, J.C.; Pope, D.J. Application of offshore breakwaters to the UK: A case study at Elmer0Bbeach. *J. Coast. Res.* **2000**, *16*, 172–187.
62. Komar, P.D. Coastal Erosion in Response to the Construction of Jetties and Breakwaters. In *Handbook of Coastal Processes and Erosion*; CRC Press: Boca Raton, FL, USA, 1983; pp. 191–204.
63. Nummedal, D.; Sonnenfeld, D.L.; Taylor, K. Sediment Transport and Morphology at the Surf Zone of Presque Isle, Lake Erie, Pennsylvania. In *Developments in Sedimentology*; Greenwood, B., Davis, R.A., Eds.; Elsevier: Amsterdam, The Netherlands, 1984; Volume 39, pp. 99–122.
64. Zaker, N.H.; Etemad-Shahidi, A. Sedimentation in Babolsar and Pozm fishery ports in Iran. In Proceedings of the 8th International Coastal Symposium (ICS 2004), Santa Catarina, Brazil, 14–19 March 2004; pp. 424–427.
65. Belknap, D.F.; Kraft, J.C. Influence of antecedent geology on stratigraphic preservation potential and evolution of Delaware's barrier systems. *Mar. Geol.* **1985**, *63*, 235–262. [CrossRef]
66. Riggs, S.R.; Cleary, W.J.; Snyder, S.W. Influence of inherited geologic framework on barrier shoreface morphology and dynamics. *Mar. Geol.* **1995**, *126*, 213–234. [CrossRef]

67. Thieler, E.R.; Brill, A.L.; Cleary, W.J.; Hobbs, C.H.; Gammisch, R.A. Geology of the Wrightsville Beach, North Carolina shoreface: Implications for the concept of shoreface profile of equilibrium. *Mar. Geol.* **1995**, *126*, 271–287. [CrossRef]
68. Hayes, M.O. General morphology and sediment patterns intidal inlets. *Sediment. Geol.* **1980**, *26*, 139–156. [CrossRef]
69. van Gaalen, J.F.; Tebbens, S.F.; Barton, C.C. Longshore sediment transport directions and rates from Northern Maine to Tampa Bay, Florida: Literature compilation and interpretation. *J. Coast. Res.* **2016**, *32*, 1277–1301. [CrossRef]
70. Fisher, J.J. *Coastal Structures in Rhode Island*; Walker, H.J., Ed.; The GeoJournal Library; Springer: Dordrecht, Netherlands, 1988; pp. 560–571.
71. McMaster, R.L. Mineralogy as an indicator of beach sand movement along the Rhode Island shore. *J. Sediment. Res.* **1960**, *30*, 404–413.
72. Boothroyd, J.C. Toward a sediment budget for the southern Rhode Island shoreline. In Proceedings of the Northeastern Section Geological Society of America, Springfield, MA, USA, 25–27 March 2002; p. 78.
73. Morton, R.A.; Bohlen, W.F.; Aubrey, D.G.; Miller, M.C. *Changes at Misquamicut Beach Rhode Island, 1962–1973*; Miscellaneous paper CERC-84-12; Coastal Engineering Research Center: Vicksburg, MS, USA, 1984.
74. Nixon, S.W.; Granger, S.; Oviatt, C.; Fields, L.; Mercer, J. *Spatial and Temporal Variability of Surface Chlorophyll, Primary Production, and Benthic Metabolism in Rhode Island and Block Island Sounds Technical Report 9: Rhode Island Ocean Special Area Management Plan*; Rhode Island Coastal Resources Management Council and University of Rhode Island Coastal Resources Center: Narragansett, RI, USA, 2010.
75. U.S. Army Corps of Engineers, N.E.D. *Point Judith Harbor of Refuge and Point Judith Pond, Narragansett, Rhode Island, Detailed Project Report and Environmental Assessment*. 2018. Available online: https://www.nae.usace.army.mil/Portals/74/docs/Topics/PtJudith107/01-PtJudith107-DraftDPR-Sept2018.pdf?ver=2018-09-19-123339-400 (accessed on 30 October 2020).
76. Walton, T.L.; Bruno, R.O. Longshore transport at a detached breakwater, phase II. *J. Coast. Res.* **1989**, *5*, 679–691.
77. Patch, K.; Griggs, G.B. *Development of Sand Budgets for California's Major Littoral Cells Eureka, Santa Cruz, Southern Monterey Bay, Santa Barbara, Santa Monica (including Zuma), San Pedro, Laguna, Oceanside, Mission Bay, and Silver Strand Littoral Cells*; Institute of Marine Sciences, Department of Boating and Waterways California Coastal Sediment Management Work Group: Santa Cruz, CA, USA, 2007.
78. Li., H.; Lin, L.; Lu, C.; Shak, A. Evaluation of breakwaters and sedimentation at dana point harbor, CA. In Proceedings of the Coastal Sediments '11, Miami, FL, USA, 2–6 May 2011.
79. Hoyt, W.H. Processes of Sedimentation and Geologic History of the Cape Henlopen/Breakwater Harbor Area, Delaware. 1983. Available online: https://elibrary.ru/item.asp?id=7363849 (accessed on 30 October 2020).
80. Pratt, J.C. *Cape Henlopen Spit Complex and Recent Evolution of Breakwater Harbor, Lewes, Delaware; M.S.*; University of Delaware: Newark, Delaware, 2007.
81. Demarest, J. *The Shoaling of Breakwater Harbor, Cape Henlopen Area, Delaware Bay, 1842 to 1971*; Sea Grant Report, Delaware SeaGrant Report DEL-SG-1-78; Delaware SeaGrant: Newark, DE, USA, 1978.
82. Schwab, W.C.; Baldwin, W.E.; Hapke, C.J.; Lentz, E.E.; Gayes, P.T.; Denny, J.F.; List, J.H.; Warner, J.C. Geologic evidence for onshore sediment transport from the inner continental shelf: Fire Island, New York. *J. Coast. Res.* **2013**, *29*, 526–544. [CrossRef]
83. Niedoroda, A.W.; Swift, D.J.P. Maintenance of the shoreface by wave orbital currents and mean flow: Observations from the Long Island Coast. *Geophys. Res. Lett.* **1981**, *8*, 337–340. [CrossRef]
84. Klinger, J.P. *Sedimentary environments and processes on the Charlestown-Green Hill Barrier/Headland shoreface and Misquamicut Barrier/Headland shoreface, south coast of Rhode Island: M.S.*; University of Rhode Island: Kingston, RI, USA, 1996.
85. Birkemeir, W.A. Field data on seaward limit of profile change. *J. Waterw. Port Coast. Ocean Eng.* **1985**, *111*, 598–602. [CrossRef]
86. Brutsche, K.E.; Rosati, J., III; Pollack, C.E.; McFall, B.C. *Calculating Depth of Closure Using WIS Hindcast Data*; U.S. Army Engineer Research and Development Center, Coastal and Hydraulics Laboratory; U.S. Army Corps of Engineers: Washington, DC, USA, 2016.

87. Hallermeier, R.J. A profile zonation for seasonal sand beaches from wave climate. *Coast. Eng.* **1981**, *4*, 253–277. [CrossRef]
88. Tait, J.F.; Ferrand, E.A. Chapter 6—Observations of the Influence of Regional Beach Dynamics on the Impacts of Storm Waves on the Connecticut Coast During Hurricanes Irene and Sandy. In *Learning from the Impacts of Superstorm Sandy*; Bennington, J.B., Farmer, E.C., Eds.; Academic Press: Boston, MA, USA, 2015; pp. 69–88. [CrossRef]